Hindawi
Journal of Nanomaterials
Volume 2018, Article ID 8678519, 8 pages
https://doi.org/10.1155/2018/8678519

Research Article

Sputtered PdO Decorated TiO_2 Sensing Layer for a Hydrogen Gas Sensor

Jeong Hoon Lee,[1] **Seungmin Kwak**,[1,2] **Jin-Hyung Lee**,[2] **Inho Kim**,[3,4] **Yong Kyoung Yoo**,[1] **Tae Hoon Lee**,[1] **Young-Seok Shim**,[5] **Jinseok Kim**,[2] **and Kyu Hyoung Lee**[6]

[1]*Department of Electrical Engineering, Kwangwoon University, Seoul 01897, Republic of Korea*
[2]*Korea Institute of Science and Technology (KIST), Seoul 02792, Republic of Korea*
[3]*R&D Center, Maccon IT Inc., Bucheon 14441, Republic of Korea*
[4]*Department of Chemical Engineering, Ajou University, Suwon 16499, Republic of Korea*
[5]*School of Electrical and Electronic Engineering, Nanyang Technological University, Singapore 639798*
[6]*Department of Materials Science and Engineering, Yonsei University, Seoul 03722, Republic of Korea*

Correspondence should be addressed to Kyu Hyoung Lee; khlee2018@yonsei.ac.kr

Received 21 September 2017; Revised 26 January 2018; Accepted 18 February 2018; Published 10 April 2018

Academic Editor: Wentao Wang

We report a sputtered PdO decorated TiO_2 sensing layer by radiofrequency (RF) sputtering methods and demonstrated gas sensing performance for H_2 gas. We prepared sputtered anatase TiO_2 sensing films with 200 nm thickness and deposited a Pd layer on top of the TiO_2 films with a thickness ranging from 3 nm to 13 nm. Using an in situ TiO_2/Pd multilayer annealing process at 550°C for 1 hour, we observed that Pd turns into PdO by Auger electron spectroscopy (AES) depth profile and confirmed decorated PdO on TiO_2 sensing layer from scanning electron microscope (SEM) and atomic-force microscope (AFM). We also observed a positive sensing signal for 3, 4.5, and 6.5 nm PdO decorated TiO_2 sensor while we observed negative output signal for a 13.5 nm PdO decorated one. Using a microheater platform, we acquired fast response time as ~11 sec and sensitivity as 6 μV/ppm for 3 nm PdO under 33 mW power.

1. Introduction

Hydrogen gas (H_2) is considered a promising future energy source and has numerous applications in industry, such as chemical production, automobiles, and fuel cells. The use of H_2 gas involves dangers associated with hydrogen storage and operation because of the high risk of explosion at H_2 concentrations greater than 4% (lower explosive limit (LEL)) in air [1]. However, H_2 gas detection has been difficult without specialized equipment because H_2 gas is odorless, tasteless, and colorless. The general techniques of H_2 gas sensing, such as gas chromatography and mass spectroscopy, have several limitations such as slow response, large system size, low portability, and high cost.

To detect H_2 gas, the sensing system requires a small size, rapid response, and high portability, sensitivity, and selectivity. Many attempts have been made to develop gas sensor devices based on ceramic-based metal-oxide sensors, two-dimensional (2D) material-based sensors, mixed composite structures, structures decorated with second-phase particles, and metal-oxide–graphene based gas sensors [2]. While the nano-material-based hydrogen gas sensor possesses a great sensing performance, the metal-oxide sensors are good candidates for commercializing sensors since it is compatible with the commercial CMOS (complementary metal-oxide semiconductor) process. As such, one could easily realize small/portable sensors with signal processing. N-type semiconductors for metal-oxide gas sensors, such as SnO, ZnO, TiO_2, and WO_3, have been used under normal atmospheric conditions and typical working temperatures in the 200–400°C range [3, 4]. There have been many reports of sensitivity enhancement by modifying the design of noble metals, such as platinum (Pt), gold (Au), palladium (Pd), and silver (Ag) [5, 6]. Favier et al. reported that the sensor

response appears to involve the closing of nanoscopic gaps caused by the dilation of Pd grains undergoing hydrogen absorption; therefore, Pd could be a favorable candidate for H_2 gas sensing [7]. Pd nanoparticles (5–20 nm) have also been reported in the sensing layer of surface acoustic wave (SAW) devices for detecting H_2 [8].

A change in the metal-oxide resistance results from a gain of surface electrons following the reaction of hydrogen with adsorbed oxygen. The TiO_2 films have been investigated by introducing different dopants such as Pt, carbon nanotubes (CNT), and Pd. It has been reported that the catalyst, such as Pt and Pd, favorably absorbs H_2 molecules and, in turn, dissociates into hydrogen atoms that diffuse to the surface of the metal-oxide (spillover process).

To fabricate a sensing layer, a sol-gel Pt/TiO_2 film [9] and Pd/TiO_2 by anodic oxidation Ti plate and sputtered Pd [1] was fabricated. For $Pd/TiO_2 : Al$, titanium metal was treated with an arc furnace and used with e-beam evaporation for Schottky contacts [10]. A TiO_2 thick film was placed in a dip coating by a H_2PtCl_6 solution for Pt/TiO_2 [11]. An electrodeposited PdNi–Si has been reported for $Pd_{0.71}Ni_{0.29}$ [12]. A graphene/zinc oxide (ZnO) nanocomposite was also reported [13]. For nanotube fabrication, TiO_2-nanotubes are generally fabricated by anodizing a titanium sheet [3, 14]. More recently, a Pd-loaded SnO_2 particle was synthesized using a sol-gel SnO_2 and Pd impregnation technique [4]. The hydrogen sensor of the Pd-decorated tubular TiO_2 layer was prepared by anodization with patterned electrodes on the SiO_2/Si substrate [15]. SnO_2- and TiO_2-based gas sensors are widely used due to its low cost, long-term stability, and high sensitivity to hydrogen gas. It has been reported that the change in electric resistance of the gas sensing layer is caused from the surface reaction between the adsorbed oxygen species and target gas. Many fabrication processes have been reported for H_2 gas sensing; however, the deposition of the sensing layer has been restricted to the wet process such as sol-gel, electrodeposition, and electroplating, in which large-area uniformity and low power consumption are difficult to achieve.

In this study, in order to overcome the previous limitation, we fabricated the highly sensitive H_2 sensors with the physical vapor deposition process, which is compatible with the commercial CMOS process. Moreover, we reduced the power consumption by forming the sensing materials on MEMS platform.

2. Materials and Methods

2.1. Sensing Layer Deposition. For the sensing layer, we loaded samples into a high-vacuum sputtering chamber through a load-lock transfer system which allows deposition on a series of thin films without venting the main chamber. Firstly, TiO_2 layer was deposited on selected area in MEMS platform by a magnetron reactive sputter at a constant target DC power of 500 W until the thickness of TiO_2 film reached approximately 200 nm. Then, Pd thin film (0, 3, 4.5, 6.5, and 13 nm) was deposited on TiO_2 film. The process pressure was approximately 6×10^{-3} mTorr. After a multilayer deposition, we annealed the TiO_2/Pd multilayered samples in an atmospheric environment tube furnace at 550°C for 1 hour to crystalize the TiO_2 films and change Pd film to PdO NPs (nanoparticles). Finally, we acquired PdO NPs decorated TiO_2 sensing layer.

2.2. Sensing Layer Characterization. The microscopic images of the device and thin films were characterized by a field emission scanning electron microscope (FE-SEM; Nova SEM, FEI), atomic-force microscope (AFM; XE-100, Park Systems), and X-ray diffraction (XRD; DMAX 2500, Rigaku). In order to measure the film thickness of PdO with several nanometer thicknesses, we used the depth profile from the Auger electron spectroscopy (AES) of PdO deposited on to the TiO_2 film. The depth profile from the AES of PdO deposited with (a) 3, (b) 4.5, (c) 6.5, and (d) 13 nm on to the TiO_2 film thickness of the PdO film was converted from the sputtering time using AES's sputtering rate of 3.3 nm/min. We calculated film thickness from the sputtering time when Pd changed to Ti.

2.3. Hydrogen Sensing Performance on Microheater. To test hydrogen gas sensing performance, we prepared the MEMS gas sensor that formed on a SiN_x membrane using a bulk micromachining technique. The device consisted of a heating electrode (Pt, 200 nm), insulating layer, sensing electrode Pt (150 nm), and sensing layer of TiO_2 (20 nm)/PdO (3–13 nm). We designed a reaction chamber of gas sensing system with a volume of 8.4 liters and injected hydrogen gas with the prepared volume to meet the desired concentration using a sample dilution of hydrogen gas in the reaction chamber. The gas in the reaction chamber was circulated with an electric fan. We measured the heating profiles using an infrared camera (MobIR® M8 IR Thermographic Camera).

3. Results and Discussion

Figure 1 shows the XRD patterns of the (a) TiO_2 films and (b) PdO NPs decorated TiO_2 film with four PdO different thicknesses. In Figure 1(a), the XRD patterns exhibited strong diffraction peaks at 25.4° and 48° which indicated the main peaks of the anatase (101). We calculated the average grain size of the TiO_2 using XRD peak broadening based on the Scherrer formula [16]. The observed particle size of 200 nm thick TiO_2 thin film layer was a nanometer scale of approximately 4.8 nm. Figure 1(b) demonstrates the XRD patterns of the PdO NPs decorated TiO_2 film with different PdO thicknesses ranging from 0 to 13 nm. We deposited in situ TiO_2 and Pd by using magnetron reactive sputtering and annealed TiO_2/Pd multilayered samples in an atmospheric environment tube furnace at 550°C for 1 hour. After the annealing process, we confirmed the formation of PdO (index: red diamond in Figure 1(b)). When the thickness of PdO increased, the main peak of PdO $2\theta = 33.8°$ was also increased, which indicated an improvement in the crystallization of the PdO thin films. A clear detectable peak of the PdO phase can be observed in the XRD pattern, even at 3 nm PdO thickness. Lallo et al. claimed that the Pd oxidation condition depends on the amount of deposited Pd. Thicker Pd deposits behaved similarly to bulk Pd samples, whereas the oxidation temperatures may be

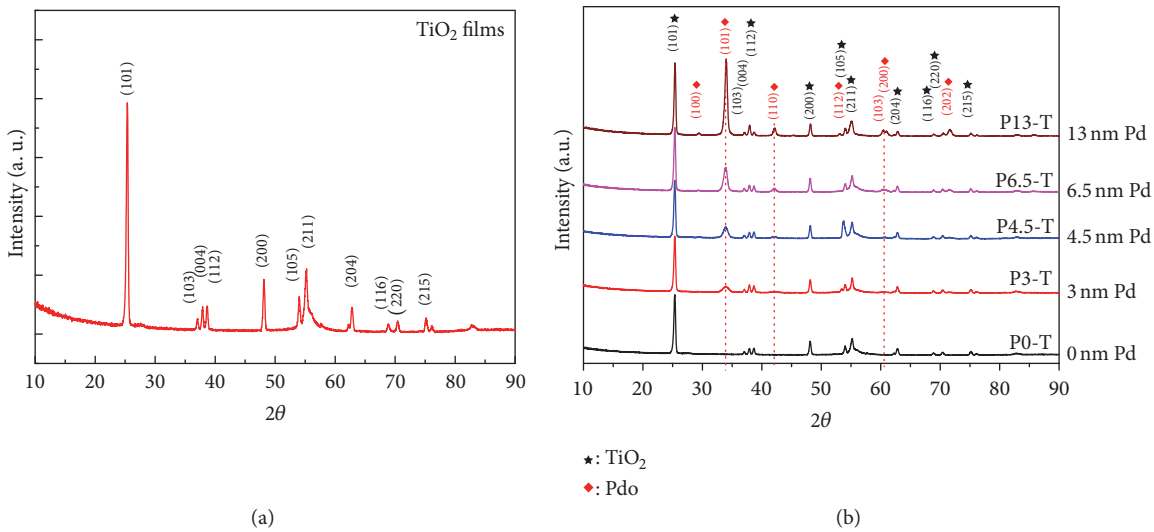

FIGURE 1: The XRD patterns of (a) TiO_2 films and (b) PdO NPs decorated TiO_2 film with four PdO different thicknesses.

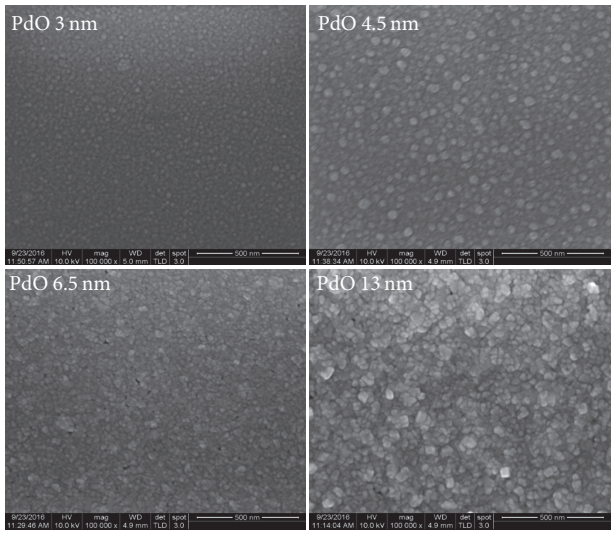

FIGURE 2: The SEM images of the PdO NPs decorated TiO_2 film (PdO thickness: 3, 4.5, 6.5, and 13 nm).

reduced for thinner films [17]. We confirmed that the Pd films after annealing at 550°C for 1 hour were completely oxidized to PdO.

The SEM images of the PdO NPs decorated TiO_2 film are shown in Figure 2. The film thickness was calculated as 3.0, 4.5, 6.5, and 13 nm using a depth profile from the AES (see Figure 4). We clearly observed grain growth with an increase in the PdO film thickness. It is generally accepted that the presence of PdO (or Pd) particles or films is essential to achieve high sensitivity for H_2 gas sensing. After a 3 nm deposition, we observed clear PdO grain formation on the TiO_2 films, and the grain size increased with the PdO thickness. The grain size and surface roughness of the PdO/TiO_2 surface were also examined using AFM, as shown in Figure 3. The root mean square (RMS) roughness linearly increased with PdO thickness. AFM observations showed that the RMS roughness increased with the PdO film thickness.

Generally, Pd thin films (<10 nm) are changed to PdO nanoparticles during the annealing. The size of nanoparticles is dependent on initial thin film thickness. In addition, size and distribution of Pd nanoparticles affect gas sensing properties by changing the current path and forming depletion region. Valden et al. [18] have reported that the cluster diameter of Au NPs affects the catalytic activity, and Zhang and Colbow reported catalytic effects of Ag NPs as a function of the initial Ag film thickness [19].

Regarding PdO NPs effects on the TiO_2 sensing layer, it is generally reported that PdO strongly affects the gas sensing properties of the metal-oxide due to their catalytic effect such as electronic and chemical sensitizations [20–22]. The distribution and size of PdO, therefore, are a critical factor to enhance the gas sensing properties. When small size PdO nanoparticles were presented, only a limited portion of the surface has a depleted region by aforementioned electronic sensitization. Meanwhile, when large size PdO clusters are represented on TiO_2 films, the effect of H_2 adsorbates was reduced since chemical sensitization was generated at three regions (metal-oxide, catalysts, and gas). Therefore, optimal dispersion of the PdO NPs allows the depleted region of the TiO_2 surface and the influence of the catalyst to extend throughout the entire surface of the semiconductor; in turn, it enables high sensitive properties to H_2 gas.

We expected that optimal dispersion of the PdO nanoparticles was acquired with PdO thickness range from 3 to 6.5 nm. Interestingly, with PdO films thickness of 13 nm, we observed different gas response signal.

Figure 4 exhibits the depth profile from the AES of PdO thickness of (a) 3, (b) 4.5, (c) 6.5, and (d) 13 nm on the TiO_2 film. The thickness of the PdO film was converted from the sputtering time using the AES's sputtering rate of 3.3 nm/min. We confirmed film thickness from AES depth profile and

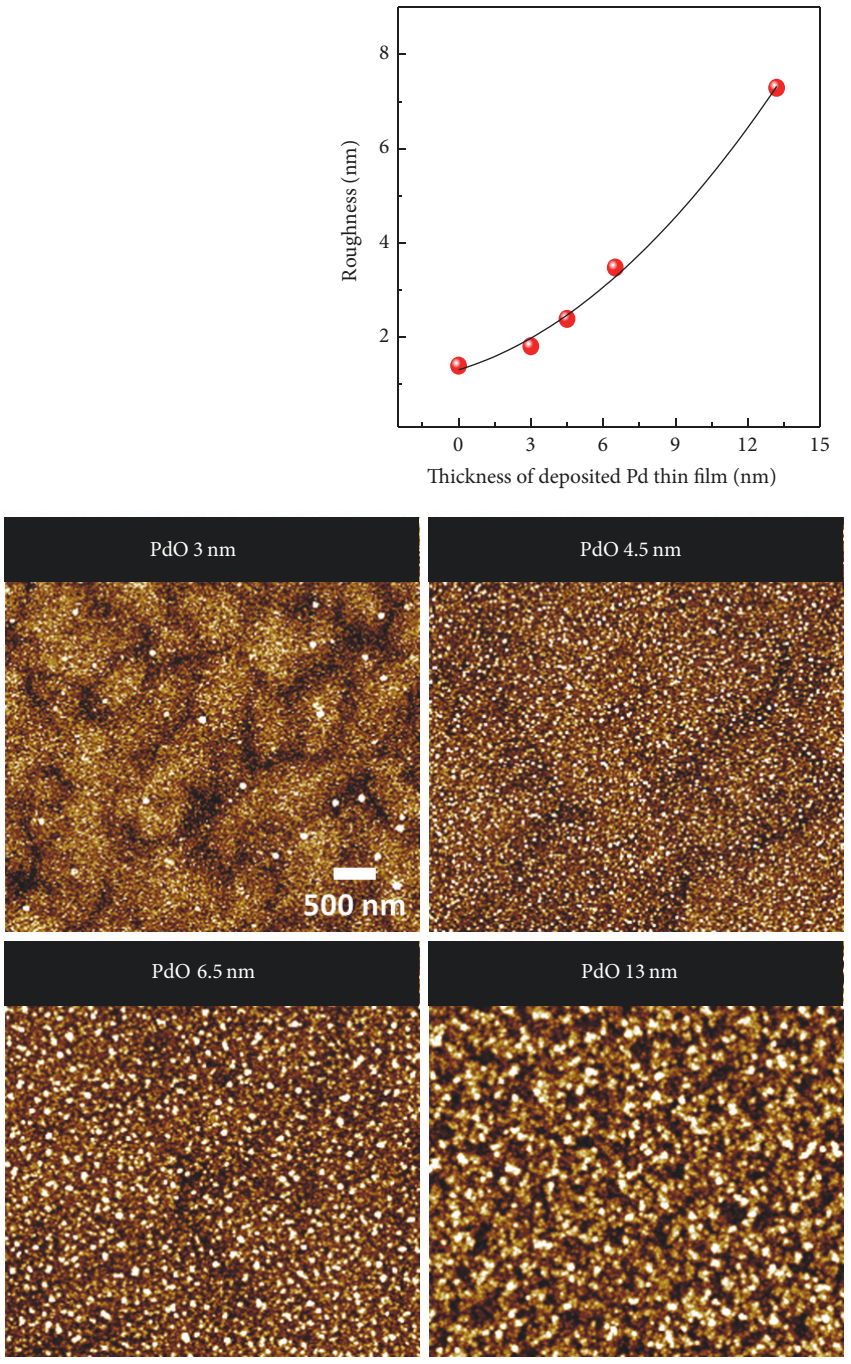

FIGURE 3: The graph of RMS surface roughness along with different PdO thickness and AFM images of PdO NPs decorated TiO_2 film.

calculated the interface of PdO and TiO_2 which was 3, 4.5, 6.5, and 13 nm, respectively. After deposition of the Pd thin film, we annealed the Pd/TiO_2 films at 550°C for 1 hour in an air atmosphere and acquired the PdO NPs decorated TiO_2 films.

The schematic three-dimensional structure of the proposed MEMS-based gas sensor is shown in Figure 5. For fabricating MEMS-based gas sensor, using low pressure chemical vapor deposition process (LPCVD), we deposited a SiN_x film (2 μm thick) on a p-type Si (100) substrate. Then we deposited 200 nm thick Pt film that was used for microheater. Note that a 10 nm thick Ti film was used for adhesion layer to increase the adhesion properties between SiN_x and Pt. The Pt heater was patterned using standard photolithography and then etched using reactive ion etcher (RIE). Here, we used an ONO insulating layer made of a SiO_2 (500 nm)/SiN_x (250 nm)/SiO_2 (250 nm) structure on Pt heater to acquire thermal stability and mechanical stability

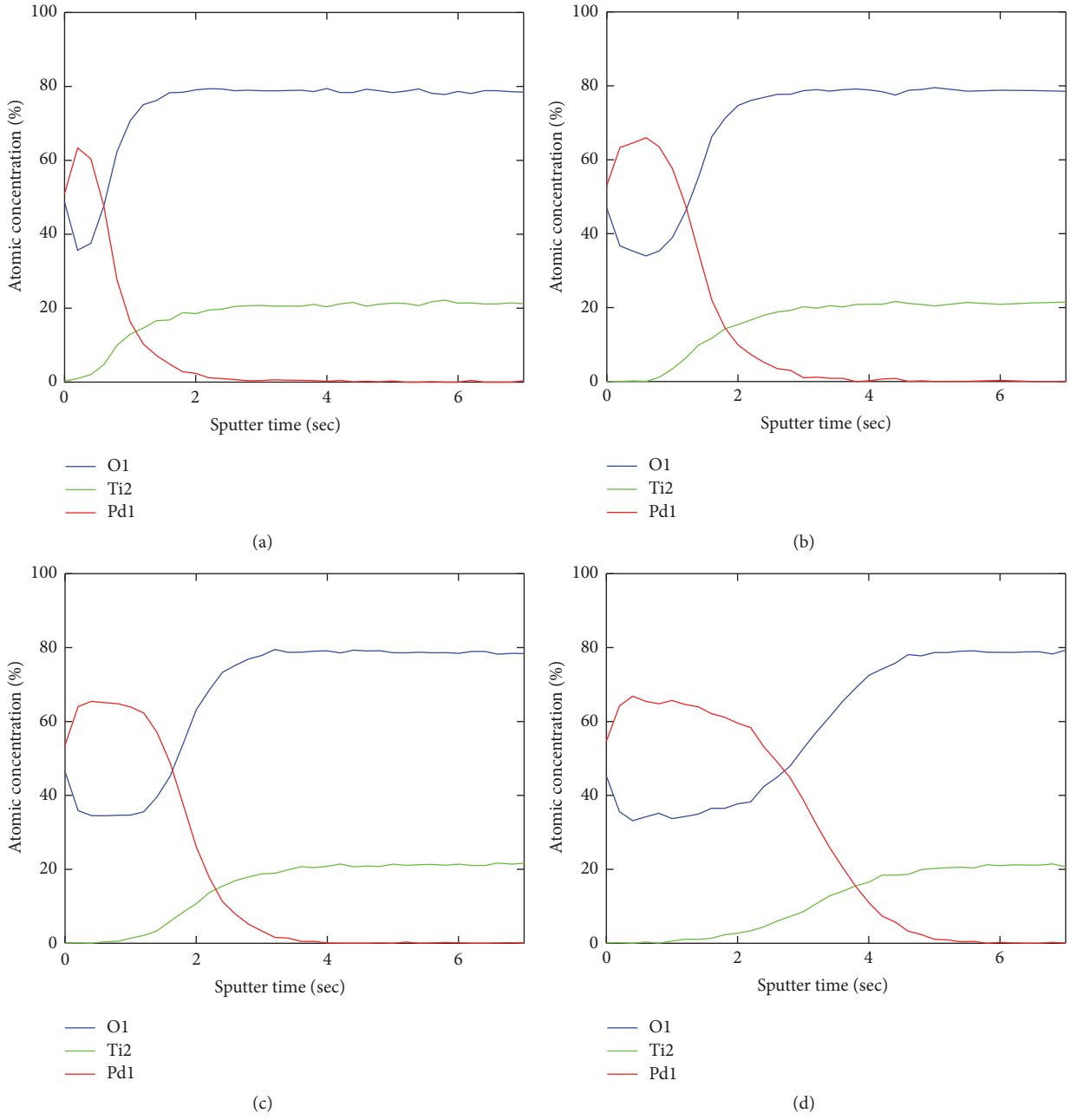

FIGURE 4: The depth profiles from Auger electron spectroscopy (AES) of PdO decorated TiO_2 films with different PdO thickness of (a) 3, (b) 4.5, (c) 6.5, and (d) 13 nm. The thickness of PdO film was converted from the sputtering time using the AES's sputtering rate of 3.3 nm/min.

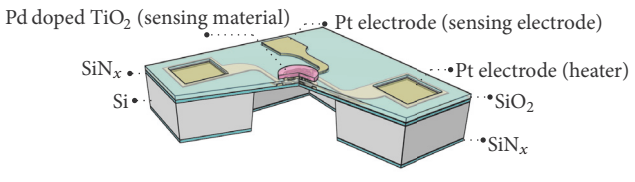

FIGURE 5: The schematic three-dimensional structure of the MEMS-based gas sensor.

that are important in the temperature rising/falling process. Note that we deposited ONO insulating layer using plasma-enhanced chemical vapor deposition (PECVD) for acquiring low residual stress and good adhesion. After annealing the multilayer films at 500°C, contact holes of Pt heater were formed using the STS AOE Deep Reactive Ion Etch (DRIE). For the sensing electrode, Pt/Ti (150 nm/30 nm thick) inter-digitated electrodes (IDEs) with the 20 μm interspacing between fingers were fabricated. The rear SiN_x membrane window (0.8 mm × 1 mm) patterning was conducted using reactive ion etching and then the bulk silicon was wet etched

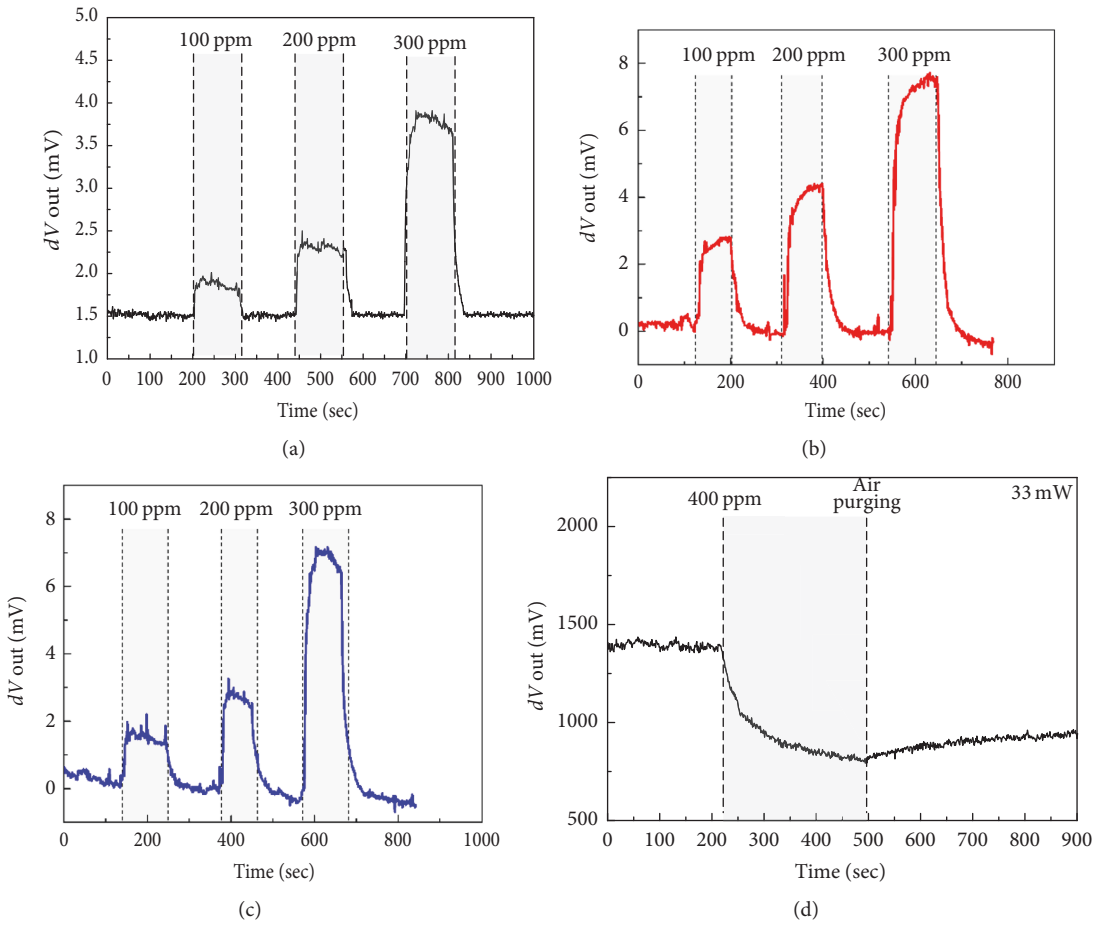

FIGURE 6: The time sequential sensor signal output with heater power consumption. The H_2 gas concentration of 100, 200, and 400 ppm was sequentially applied to the PdO decorated TiO_2 films with PdO thickness of (a) 3, (b) 4.5, (c) 6.5, and (d) 13 nm on the TiO_2 film.

with a KOH silicon etchant. Finally, we cut the wafer into unit sensors (2.5 mm × 2.5 mm) with a wafer sawing machine. When we applied voltage across the Pt heaters on unit sensors, the temperature rapidly increased and then quickly dropped when the voltage was removed.

Figure 6 shows the sensor signal output signal with four different PdO thicknesses. The H_2 gas concentrations of 100, 200, and 400 ppm were sequentially applied to the PdO NPs decorated TiO_2 films for four different PdO thickness of (a) 3, (b) 4.5, (c) 6.5, and (d) 13 nm. Without PdO layer, we observed no significant output (see Supplementary Materials: Figure S2). We applied dc field to microheater and power consumption was 33 mW. Low power consumption is an essential criterion for portable IoT (Internet of things) applications. We designed the optimal microheater with a line width of 60 μm and calculated the power consumption to be 33 mW at 2.0 V (see Supplementary Materials: Figure S1). When voltage was applied to the microheater, the temperature increased because it converted electrical energy to thermal energy. Regarding the temperature with applied voltage using an infrared camera, the microheater allowed a high coefficient of temperature increase of 5.7°C/mW. We conducted all the experiments under humidity conditions of 45 ± 2.5%. With the increase of H_2 gas of 100, 200, and 400 ppm concentrations, the output signals of the sensors linearly increased with H_2 gas concentration for the 3, 4.5, and 6.5 nm thick PdO on TiO_2 film gas sensor (Figures 6(a)–6(c)) and we observed a fast response of H_2 for the 3, 4.5, and 6.5 nm thick PdO. For 3 nm PdO, we calculated response time as 11 sec at 33 mW. Note that we estimated the response time for signals that reached 90% of the mean baseline value of the detection signal [23]. We determined that the power of 33 mW also corresponded to a surface temperature of approximately 150°C. By increasing input power, surface temperature increases, which then increases sensor output and response time. We determined the sensor sensitivity (the slope of the sensor output voltage versus H_2 concentration) to check the effects of temperature on sensitivity. For 3 nm PdO NPs decorated TiO_2 sensing layer, under the operating temperature of 150°C (33 mW), the sensitivity was calculated as 6 μV/ppm. Interestingly, in cases with a 13.5 nm PdO decorated TiO_2 sensor (Figure 6(d)), the sign of the output signal was negative. Moreover, we observed that the response time and recovery time also required significantly more time compared with 3, 4.5, and 6.5 nm thick PdO on TiO_2 film. The Pd deposition has been reported to effectively improve

the hydrogen sensing abilities of the sensor because of the catalytic effect of Pd [24]. The catalyst, such as Pt and Pd, favorably absorbed the H_2 molecules, which then dissociated into H atoms that diffused to the surface of the metal-oxide (spillover process) [25]. For 13.5 nm thick Pd film, we expect that they did not change to discontinuous NPs; in turn, they still fully covered TiO_2 film surface, leading to inactive TiO_2 surface to H_2 gas. In the case of the PdO layer with a thickness of 13.5 nm, the sensing layer acts as a sensing layer, not a catalyst layer, so that the sensing signal appears to be opposite to that of the PdO layer having a thickness of 3, 4.5, and 6.5 nm.

The H_2 sensing mechanisms of Pd- (PdO-) based sensors can be classified into two categories [26]. Firstly, in case of presenting of nanogap structure (discontinuous structure), when a Pd structure is exposed to H_2, a Pd/H solid solution is formed at low H_2 concentrations. At high concentrations of H_2, there is a 3.5% volume expansion due to the numerous H atoms incorporated into Pd. Since nanogaps in Pd structures interfere with electric current flow, volume expansion after H_2 exposure allows the nanogaps to be closed, leading to a substantial inflow of electrical current. As a result, the electrical resistance (conduction) of H_2 sensors abruptly decreases (increases) when exposed to H_2 and recovers to the initial base resistance (base conduction is zero) after removal of H_2. Secondly, in contrast to presenting nanogap, H atoms can be incorporated into the continuous Pd structures and act as electron scattering sources, so that electrical resistance increases. In this case, the electrical resistance increases with increase in H_2 concentration, because the frequency of electron-H scattering increases as the amount of H atoms in the Pd structures increases.

4. Conclusion

To conclude, our findings provide a methodology for the deposition of H_2 sensing thin films of PdO NPs decorated TiO_2 films using sputtering. Subsequent thin film characterization using XRD, SEM, AFM, and AES depth profiles was used to observe the deposition parameters for PdO NPs decorated TiO_2 films. It was found that the sputtering thickness of the catalytic PdO layer greatly influenced the surface morphology, which resulted in gas sensing properties. We acquired the sensitivity as $+6\,\mu$V/ppm for 3 nm PdO decorated TiO_2 sensor under 33 mW power consumption while the sign of the output signal was negative for 13.5 nm PdO decorated TiO_2 sensor.

Conflicts of Interest

The authors declare that there are no conflicts of interest regarding the publication of this paper.

Authors' Contributions

Jeong Hoon Lee and Seungmin Kwak have equally contributed to this paper.

Acknowledgments

This work was supported by a National Research Foundation of Korea grant funded by the Korean government (MEST; NRF-2015R1D1A1A01059806) and by a grant of the Korea Health Technology R&D Project through the Korea Health Industry Development Institute (KHIDI), funded by the Ministry of Health and Welfare, Republic of Korea (Grant no. HI16C0272). The work reported in this paper was conducted during the sabbatical year of Kwangwoon University in 2015.

Supplementary Materials

Supplementary information for this article can be found in the attached file. Figure S1: (a) IR measurement set-up and (b) measured temperature by IR camera as function of applied voltage. Figure S2: hydrogen gas detection without PdO layer. *(Supplementary Materials)*

References

[1] A. Mirzaei, S. G. Leonardi, and G. Neri, "Detection of hazardous volatile organic compounds (VOCs) by metal oxide nanostructures-based gas sensors: A review," *Ceramics International*, vol. 42, no. 14, pp. 15119–15141, 2016.

[2] Z. Dai, L. Xu, G. Duan et al., "Fast-response, sensitivitive and low-powered chemosensors by fusing nanostructured porous thin film and IDEs-microheater chip," *Scientific Reports*, vol. 3, article no. 1669, 2013.

[3] C. Rossi, E. Scheid, and D. Estève, "Theoretical and experimental study of silicon micromachined microheater with dielectric stacked membranes," *Sensors and Actuators A: Physical*, vol. 63, no. 3, pp. 183–189, 1997.

[4] Y. Cui, "Nanowire nanosensors for highly sensitive and selective detection of biological and chemical species," *Science*, vol. 293, no. 5533, pp. 1289–1292.

[5] A. Wisitsoraat, A. Tuantranont, E. Comini, G. Sberveglieri, and W. Wlodarski, "Characterization of n-type and p-type semiconductor gas sensors based on NiOx doped TiO2 thin films," *Thin Solid Films*, vol. 517, no. 8, pp. 2775–2780, 2009.

[6] H. Gu, Z. Wang, and Y. Hu, "Hydrogen gas sensors based on semiconductor oxide nanostructures," *Sensors*, vol. 12, no. 5, pp. 5517–5550, 2012.

[7] F. Favier, E. C. Walter, M. P. Zach, T. Benter, and R. M. Penner, "Hydrogen sensors and switches from electrodeposited palladium mesowire arrays," *Science*, vol. 293, no. 5538, pp. 2227–2231, 2001.

[8] D. Sil, J. Hines, U. Udeoyo, and E. Borguet, "Palladium Nanoparticle-Based Surface Acoustic Wave Hydrogen Sensor," *ACS Applied Materials & Interfaces*, vol. 7, no. 10, pp. 5709–5714, 2015.

[9] X. Bévenot, A. Trouillet, C. Veillas, H. Gagnaire, and M. Clément, "Hydrogen leak detection using an optical fibre sensor for aerospace applications," *Sensors and Actuators B: Chemical*, vol. 67, no. 1, pp. 57–67, 2000.

[10] C. Xiang, Z. She, Y. Zou et al., "A room-temperature hydrogen sensor based on Pd nanoparticles doped TiO2 nanotubes," *Ceramics International*, vol. 40, pp. 16343–16348, 2014.

[11] P. Bhattacharyya, P. K. Basu, B. Mondal, and H. Saha, "A low power MEMS gas sensor based on nanocrystalline ZnO thin

films for sensing methane," *Microelectronics Reliability*, vol. 48, no. 11-12, pp. 1772–1779, 2008.

[12] P. Bhattacharyya, "Technological journey towards reliable microheater development for MEMS gas sensors: a review," *IEEE Transactions on Device and Materials Reliability*, vol. 14, no. 2, pp. 589–599, 2014.

[13] J. H. Lee, K. S. Hwang, and T. S. Kim, "Microstress relaxation effect of Pb(Zr0.52Ti0.48) O3 films with thicknesses for micro/nanopiezoelectric device," *Applied Physics Letters*, vol. 96, no. 9, Article ID 092904, 2010.

[14] P. C. H. Chan, G.-Z. Yan, L.-Y. Sheng et al., "An integrated gas sensor technology using surface micro-machining," *Sensors and Actuators B: Chemical*, vol. 82, no. 2-3, article no. 4200, pp. 277–283, 2002.

[15] X. Chen, C. K. Y. Wong, C. A. Yuan, and G. Zhang, "Nanowire-based gas sensors," *Sensors and Actuators B: Chemical*, vol. 177, pp. 178–195, 2013.

[16] L. C. Tien, H. T. Wang, B. S. Kang et al., "Room-temperature hydrogen-selective sensing using single Pt-coated ZnO nanowires at microwatt power levels," *Electrochemical and Solid-State Letters*, vol. 8, no. 9, pp. G230–G232, 2005.

[17] J. Lallo, S. A. Tenney, A. Kramer, P. Sutter, and M. Batzill, "Oxidation of palladium on Au(111) and ZnO(0001) supports," *The Journal of Chemical Physics*, vol. 141, no. 15, Article ID 154702, 2014.

[18] M. Valden, X. Lai, and D. W. Goodman, "Onset of catalytic activity of gold clusters on titania with the appearance of nonmetallic properties," *Science*, vol. 281, no. 5383, pp. 1647–1650, 1998.

[19] J. Zhang and K. Colbow, "Surface silver clusters as oxidation catalysts on semiconductor gas sensors," *Sensors and Actuators B: Chemical*, vol. 40, no. 1, pp. 47–52, 1997.

[20] Y.-S. Shim, H. G. Moon, D. H. Kim et al., "Au-decorated WO3 cross-linked nanodomes for ultrahigh sensitive and selective sensing of NO2 and C2H5OH," *RSC Advances*, vol. 3, no. 26, pp. 10452–10459, 2013.

[21] E. Comini, G. Faglia, G. Sberveglieri, Z. Pan, and Z. L. Wang, "Stable and highly sensitive gas sensors based on semiconducting oxide nanobelts," *Applied Physics Letters*, vol. 81, no. 10, pp. 1869–1871, 2002.

[22] X. Liu, J. Zhang, T. Yang, X. Guo, S. Wu, and S. Wang, "Synthesis of Pt nanoparticles functionalized WO3 nanorods and their gas sensing properties," *Sensors and Actuators B: Chemical*, vol. 156, no. 2, pp. 918–923, 2011.

[23] K. Kalantar-Zadeh, "Sensors: An introductory course," *Sensors: An Introductory Course*, vol. 9781461450528, pp. 1–196, 2013.

[24] J. Moon, H.-P. Hedman, M. Kemell, A. Tuominen, and R. Punkkinen, "Hydrogen sensor of Pd-decorated tubular TiO_2 layer prepared by anodization with patterned electrodes on SiO_2/Si substrate," *Sensors and Actuators B: Chemical*, vol. 222, Article ID 18909, pp. 190–197, 2016.

[25] B. Liu, D. Cai, Y. Liu et al., "High-performance room-temperature hydrogen sensors based on combined effects of Pd decoration and Schottky barriers," *Nanoscale*, vol. 5, no. 6, pp. 2505–2510, 2013.

[26] J. Lee, W. Shim, J.-S. Noh, and W. Lee, "Design rules for nanogap-based hydrogen gas sensors," *ChemPhysChem*, vol. 13, no. 6, pp. 1395–1403, 2012.